energies

Article

Numerical Study on Effect of Flue Gas Recirculation and Co-Firing with Biomass on Combustion Characteristics in Octagonal Tangentially Lignite-Fired Boiler

Jiajun Du [1], Jiahui Yang [2], Yonggang Zhao [1], Qianxin Guo [1], Yaodong Da [2,3,*] and Defu Che [2]

1 Shenhua Group CFB Technology R&D Center, CFB Research and Development Department (R&D), Xi'an 710065, China; dujiajun_1983@163.com (J.D.); zhaoyonggang202311@163.com (Y.Z.); guoqianxin2023@163.com (Q.G.)
2 State Key Laboratory of Multiphase Flow in Power Engineering, School of Energy and Power Engineering, Xi'an Jiaotong University, Xi'an 710049, China; yjh123@stu.xjtu.edu.cn (J.Y.); dfche@mail.xjtu.edu.cn (D.C.)
3 China Special Equipment Inspection and Research Institute, Beijing 100029, China
* Correspondence: dayaodong@csei.org.cn

Abstract: The octagonal tangentially fired boiler can be utilized for burning lignite with high moisture. Co-firing biomass in an octagonal tangential boiler is considered a promising approach. A numerical simulation is carried out in this study to analyze the impact of flue gas recirculation (FGR) and the biomass blending ratio on heat and mass transfer in an octagonal tangentially fired boiler. When the FGR rate increases from 0 to 30%, the maximum temperature in the boiler decreases from 2162.8 to 2106.5 K. Simultaneously, the average temperature of the center longitudinal section decreases from 1589.0 to 1531.9 K. The maximum fluctuation of the outlet flue gas temperature remains within 10.9 K for the four calculated working conditions. Consequently, the efficiency of the boiler is basically unchanged. However, the flue gas temperature at the furnace outlet decreases significantly from 1605.9 to 1491.9 K. When the biomass blending ratio increases from 0 to 20%, the mean temperature of the primary combustion zone decreases from 1600.5 to 1571.2 K.

Keywords: biomass; lignite; octagonal tangentially fired boiler; flue gas recirculation; numerical simulation

Citation: Du, J.; Yang, J.; Zhao, Y.; Guo, Q.; Da, Y.; Che, D. Numerical Study on Effect of Flue Gas Recirculation and Co-Firing with Biomass on Combustion Characteristics in Octagonal Tangentially Lignite-Fired Boiler. *Energies* **2024**, *17*, 475. https://doi.org/10.3390/en17020475

Academic Editor: Eliseu Monteiro

Received: 4 December 2023
Revised: 9 January 2024
Accepted: 17 January 2024
Published: 18 January 2024

1. Introduction

The extensive utilization of fossil fuels has led to heightened environmental pollution [1] and climate change [2]. To promote sustainable development and decrease the reliance on fossil fuels, researchers have turned their attention towards alternative energy sources. Among these alternatives, biomass has emerged as a promising option. Biomass, which includes wood waste [3], crop stalks [4], and energy plants [5], is a renewable resource. During the combustion of biomass, the released amount of carbon dioxide is roughly equivalent to the amount absorbed by the plants during their growth [6]. As a result, burning biomass is regarded as a low-carbon and environmentally friendly practice. The existing crop straw in China holds a promising potential for biomass energy, approximately equivalent to 170 million tons of standard coal [7]. However, various properties of biomass, including its high moisture content [8] and ash content [9,10], have posed challenges to its widespread application in the field of boilers.

Co-firing biomass with coal has become a common practice to harness the energy potential of biomass [11]. Compared to coal-fired boilers, this practice can effectively reduce carbon emissions [12,13]. Additionally, co-firing biomass and coal can enhance combustion efficiency and stability in contrast to fully burning biomass alone [14]. Lignite is one of the target fuels that has been studied for co-combustion with biomass. Lignite, which refers to coal with a volatile content greater than 37% [15], is a typical low-rank coal [16]. Coal power generation currently accounts for around 62.6% of China's total power generation [17], with lignite reserves representing approximately 13% of China's total coal reserves [18]. Efficiently utilizing lignite could significantly alleviate China's energy constraints.

In some regions of northern China, such as Heilongjiang [19] and Inner Mongolia [20], there exists an abundance of lignite resources. Concurrently, these regions have a well-developed local agriculture industry. By implementing the co-firing of lignite and biomass in local thermal power plants, it is possible to enhance the utilization efficiency of the region's resources while simultaneously lowering the cost of power generation. However, in current research, the focus on studying lignite and biomass co-combustion is primarily on circulating fluidized bed boilers [21–23], with few studies available related to pulverized coal boilers. This is due to lignite being characterized by a low calorific value [24], high water content [25], and susceptibility to spontaneous combustion [26]. These attributes greatly limit its application in pulverized coal boilers.

A simple and viable solution involves preheating and drying the lignite [27]. The octagonal tangentially fired boiler, equipped with fan mills, is a commonly used boiler for burning lignite with a high moisture content. In this boiler design, high-temperature recirculation flue gas is mixed with air to preheat the lignite. The lignite is then dried and pulverized into coal particles in the fan mill.

To achieve an efficient and clean combustion of biomass and lignite, the co-combustion of biomass and lignite in the octagonal tangentially fired boiler with flue gas recirculation has also been studied. Nikolopoulos et al. [28] conducted a comprehensive investigation into the technical and economic viability of co-firing biomass and lignite in octagonal tangentially fired boilers. Their study utilized a computational fluid dynamics (CFD) model, which holds valuable reference significance. However, their focus was on a specific condition and they did not provide an in-depth analysis. Milicevic et al. [29] conducted a numerical simulation to examine the heat and mass transfer in the furnace under various load conditions when different types of biomasses were co-fired. The findings indicate that blended firing is an environmentally friendly combustion approach. It is worth noting that the boiler they investigated is similar to the subject of this study, making their findings highly relevant. However, it should be mentioned that their model did not consider the superheaters and reheaters, which may lead to significant discrepancies.

In the octagonal tangential boiler, flue gas recirculation technology is employed. The rate of gas recirculation plays a significant role in heat and mass transfer within the furnace. However, previous studies on this topic have commonly treated this factor as a constant value, overlooking its potential influence. In this study, using a 600 MW octagonal boiler as an example, the detailed influence of the flue gas recirculation rate and biomass blending ratio on the flow field, temperature field, and composition field in the boiler under the boiler rated load (BRL) working condition was thoroughly investigated. The research findings can serve as a reference for boiler operation adjustments.

2. Model Description

2.1. Physical Model

A 600 MW boiler burning lignite was taken as the research object in this study. The size of the furnace cross-section is 20.40 m $\times$ 20.07 m, while the distance from the bottom of the ash hopper to the ceiling is 79.75 m. Detailed information regarding the boiler's structure is illustrated in Figure 1, while Table 1 presents key parameters for reference.

Near the division platen superheater, the water-cooled wall is equipped with eight extraction openings to draw out the flue gas from furnace. The extracted flue gas is then combined with cold flue gas in front of the coal mill as a desiccant to heat and dry the coal. Subsequently, the desiccant transports the pulverized coal from the burner nozzles into the boiler for combustion.

The burners comprise three levels, with the top burners comprising a single layer of burner nozzles and the middle and bottom consisting of two layers of burner nozzles. In addition to the burner nozzles, each layer of the burner is equipped with multiple secondary air nozzles. These secondary air nozzles can be categorized into five different groups based on their shape and position, as illustrated in Figure 1c. In addition, there are four layers of separated over-fire air (SOFA) nozzles above the top burners. To facilitate the combustion process, eight columns of burner nozzles and auxiliary air nozzles are arranged on the water-cooled wall, with two columns on each of the four walls. The mixture of pulverized coal and auxiliary air enters the furnace at a specific angle and forms a tangential circle in the central region of the boiler, as shown in Figure 2.

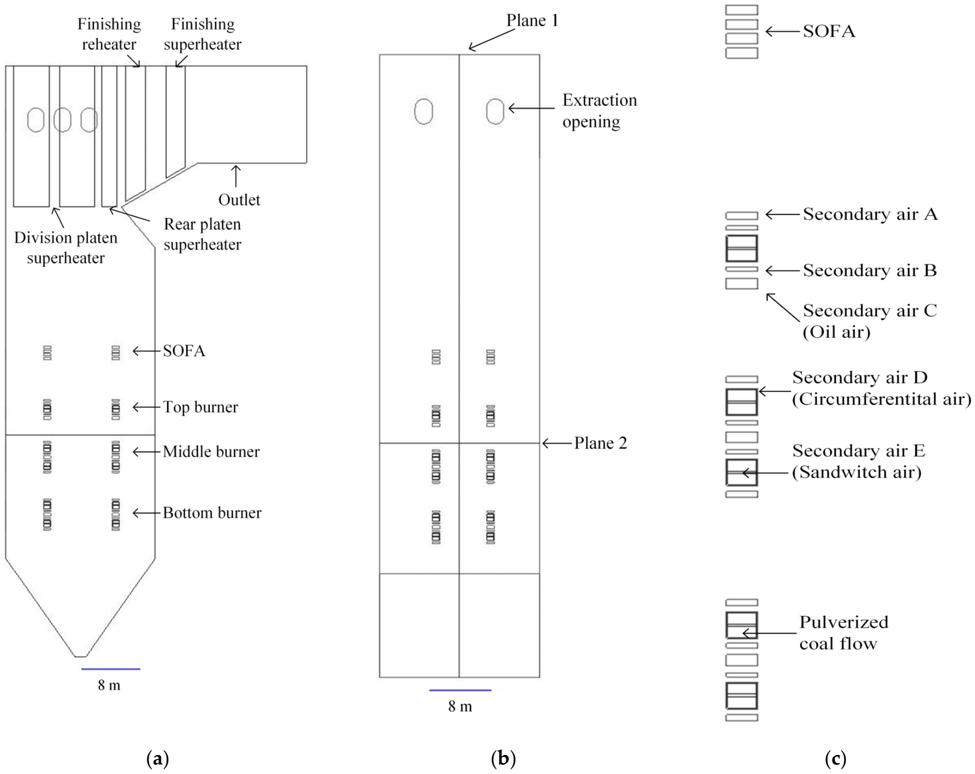

Figure 1. The structure of the boiler. (**a**) Front view. (**b**) Left view. (**c**) Types and arrangement of nozzles.

Table 1. Design parameters of the boiler.

Outlet Flow of Superheater ($t\ h^{-1}$)	Superheated SteamTempera-ture (K)	Superheated Steam Pressure (MPa)	Feed Water Temperature (K)	Exhaust Gas Temperature (K)	Outlet Excess Air Ratio	Boiler Thermal Efficiency (%)
1808.0	844.0	28.45	554.0	608.0	1.2	91.35

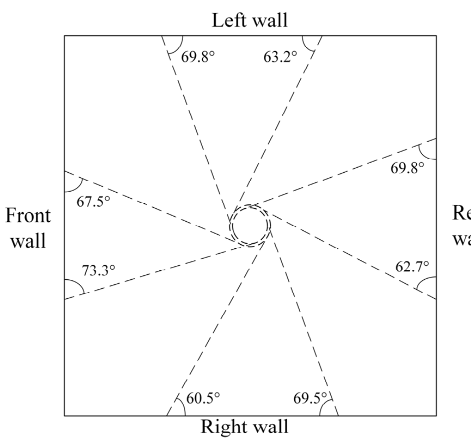

Figure 2. Air flow directions of the nozzles.

The fuel utilized in the boiler is high-moisture lignite, while corn straw is utilized as the biomass in this study. Table 2 presents the proximate analysis and elemental analysis of lignite and biomass on the as-received basis (w_{ar}). The physical properties of the fuel refer to a description in the literature [29].

Table 2. Fuel property analysis.

Fuel	Proximate Analysis (%)		Elemental Analysis (%)					$Q_{net,ar}$ (MJ kg^{-1})
	w_{ar} (A)	w_{ar} (M)	w_{ar} (C)	w_{ar} (H)	w_{ar} (O)	w_{ar} (N)	w_{ar} (S)	
Lignite	19.46	50.00	28.85	2.19	7.87	0.3	0.24	10.26
Corn straw	10.60	7.00	44.63	7.57	28.76	0.75	0.16	17.51

2.2. Numerical Model

This numerical model was developed based on Ansys Fluent 2022 R1. The mass conservation equation, energy conservation equation, and momentum equation have been considered comprehensively in the solver [30]. The Discrete-Ordinates (DO) model was employed as the radiation model. The realizable k-ε model (2 equations) was employed to calculate turbulence in this study. This model has been extensively validated for a variety of flows and significantly outperforms the standard model [31]. To calculate the chemical reaction in the combustion process, the species transport model in the species model, which can simulate the interaction between the components of the fluid mixture or with other phases, was employed and the volumetric reaction was set [30]. The two-competing-rates model and the kinetics/diffusion-limited model were used to model the devolatilization and combustion of coal particles, respectively. By activating the two corresponding models in Fluent, the calculations on the generation of thermal and fuel nitrogen oxides (NO_x) were performed. Meanwhile, the discrete phase model (DPM) should be set to simulate the coupling between the fluid and the discrete phase (pulverized coal particles). During the calculation, one DPM iteration would be performed after every 30 iterations of flow field. Two planes (Plane 1 and Plane 2) are labeled in Figure 1. The convergence conditions were that the average temperature changes of these two planes are both less than 0.1% within fifty iteration intervals.

2.3. Mesh Generation

Ansys ICEM CFD 2022 R1 software was employed for mesh generation in this study. To account for the structural characteristics of different areas, the boiler was initially divided into distinct blocks, with each block generating its own mesh. Interfaces between blocks were established to facilitate the transmission of information. All grids employed in this study were hexahedral structured grids, with the qualities consistently above 0.7.

Given that the primary combustion zone is the area where combustion predominantly occurs, a higher grid density was implemented here. To ensure that the calculation results were not affected by grid number, three meshes with grid numbers of 1.49 million, 1.95 million, and 2.52 million were employed to simulate the BRL working condition. Figure 3 illustrates the temperature variation along the vertical axis of the central line in the primary combustion zone when employing various meshes. When the grid number increases from 1.95 million to 2.52 million, the root-mean-square error (RMSE) between the two results is only 3.8 K. Hence, considering both calculation accuracy and cost, the mesh with a number of 1.95 million was adopted, as shown in Figure 4.

2.4. Boundary Conditions

In this study, all inlets were configured as mass flow inlets based on the actual mass flow. It is crucial to consider the species mass fractions of the airflow since the primary air inlet comprises a mixture of flue gas and water vapor, which is generated by the evaporation of moisture in lignite. To determine the species mass fractions of the airflow, the average mass fractions of O_2, CO_2, and other species on the surface of the extraction openings were read. Then, the proportions of various gases in the primary air were determined according to the mass of hot flue gas and lignite. The results were applied as the species mass fractions of the primary air inlets. The extraction openings were configured as mass flow outlets according to the specified flue gas extraction rate. The outlet of the boiler was set as an outflow boundary.

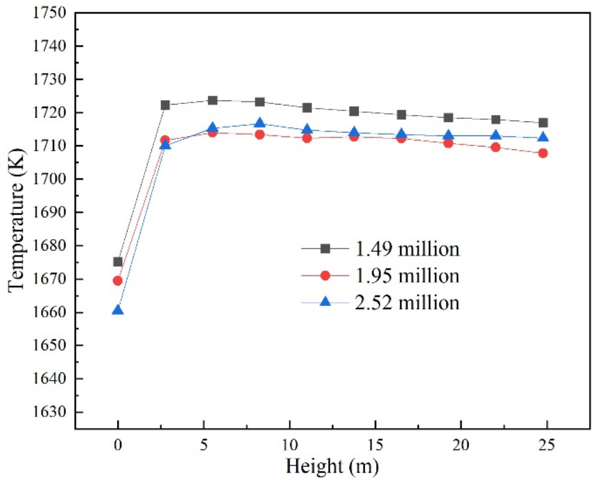

Figure 3. Temperature distribution of primary combustion zone along height direction under different grid numbers.

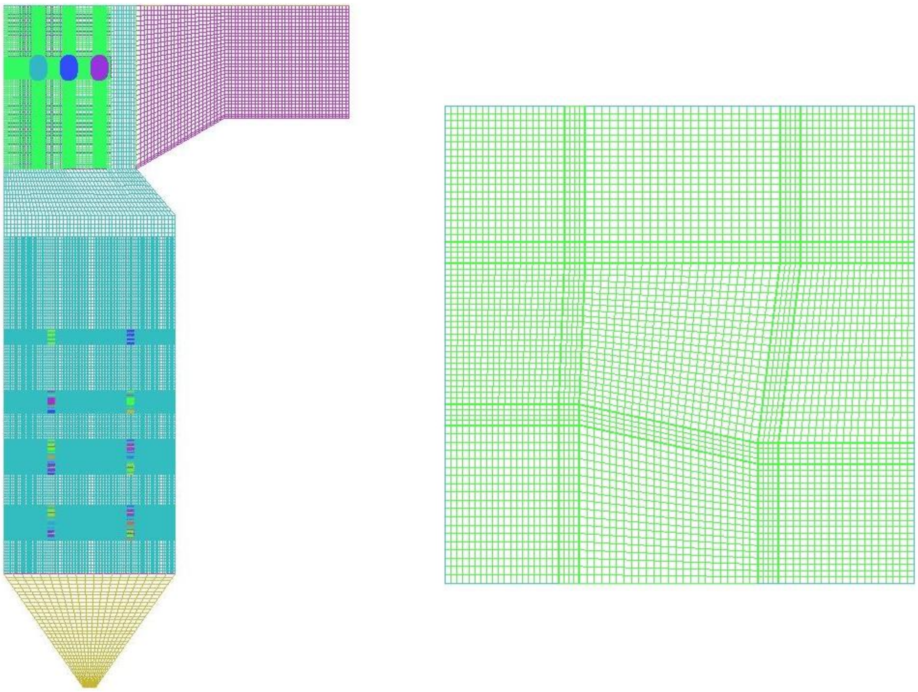

(**a**) (**b**)

Figure 4. Generated mesh. (**a**) Global mesh. (**b**) Top view of primary combustion zone.

The standard wall function, which establishes a relationship between the physical properties at the wall and those in the turbulent core region through a semi-empirical formula, was utilized as the wall function. In this model, all walls were considered isothermal, with the temperature set as the average value between the inlet and outlet fluid temperatures for each wall [32]. The temperature of each region can be found in Table 3.

Table 3. Temperature settings of each region.

Region	Water-Cooled Wall	Division Platen Superheater	Rear Platen Superheater	Finishing Reheater	Finishing Superheater
Temperature (K)	554	749	794	842	844

2.5. Simulated Working Conditions

The FGR rate (w) and biomass blending ratio (r) were considered as independent variables in this study. To simplify the model and emphasize the research focus, the following assumptions were made during the design of working conditions:

- When w changes, coal consumption and the amount of air remain constant [33].
- All the recirculating flue gas is extracted from the extraction openings and is then directed into the furnace through the primary air nozzles.
- The coal is heated into an air-drying-based state before entering the boiler. The primary air flow consists of flue gas, dry pulverized coal, and water vapor.
- When co-firing biomass, the blending ratio of each layer of burners is the same [34].

Based on the above assumptions, four working conditions with w of 0, 10%, 20%, and 30% while r = 0, and three working conditions with r of 0, 10%, and 20% while w = 20% under a 600 MW load were designed. The detailed parameter settings for each working condition are presented in Table 4. For all operating conditions, the excess air coefficient was set to 1.2, and the SOFA rate was set to 0.25. When w = 0, a small amount of air (5% of the total airflow) was added to the primary air to facilitate the entry of coal particles into the furnace.

Table 4. Parameters of the simulated working conditions.

Case Number	Flue Gas Recirculation Rate (%)	Flue Gas ($t\ h^{-1}$)	Secondary Air ($t\ h^{-1}$)	SOFA ($t\ h^{-1}$)	Coal Consumption ($t\ h^{-1}$)	Biomass Consumption ($t\ h^{-1}$)
1	0	0	1854.3	618.1	529.1	0
2	10	300.2	1854.3	618.1	529.1	0
3	20	600.3	1854.3	618.1	529.1	0
4	30	900.5	1854.3	618.1	529.1	0
5	20	587.1	1821.2	607.1	476.2	31.0
6	20	573.5	1786.7	595.6	423.3	62.0

3. Results and Discussion

3.1. Model Validation

In the actual operational data of the boiler, data similar to simulated working condition 2 in this study are selected. A smoke temperature probe is installed at the horizontal flue exit position of the boiler, corresponding to the outlet position of the numerical simulation physical model. The numerical simulation results are compared with the actual test results, revealing a mere difference of 22.0 K, specifically 1155.5 and 1177.5 K, respectively. The comparison results verify the accuracy of the numerical simulation model employed in this study.

3.2. Heat and Mass Transfer without Flue Gas Recirculation and Co-Firing

Figure 5 shows the flow field of the longitudinal section in the center of the boiler (Plane 1 in Figure 1) and the cross-section above the middle burner (Plane 2 in Figure 1) when w = 0. As can be seen from Figure 5b, the air flow forms a regular circle pattern in the middle of the boiler. In the lower region of the primary combustion zone, the air flow mainly rotates near the boiler wall, resulting in a velocity distribution pattern characterized by high velocities around the periphery and lower velocities towards the center. In the middle and upper part of the boiler, as the air inflow increases, the extent of the tangential circle expands continuously, while the speed in the central region begins to surpass that of the surrounding flow. In the primary combustion zone, the average flue gas velocity rises with height. When the flue gas flows through the furnace arch into the horizontal flue, the cross-sectional area of the flow shrinks rapidly. Meanwhile, the furnace arch plays a certain role in disrupting the flow [35]. Therefore, the velocity of the flue gas increases correspondingly.

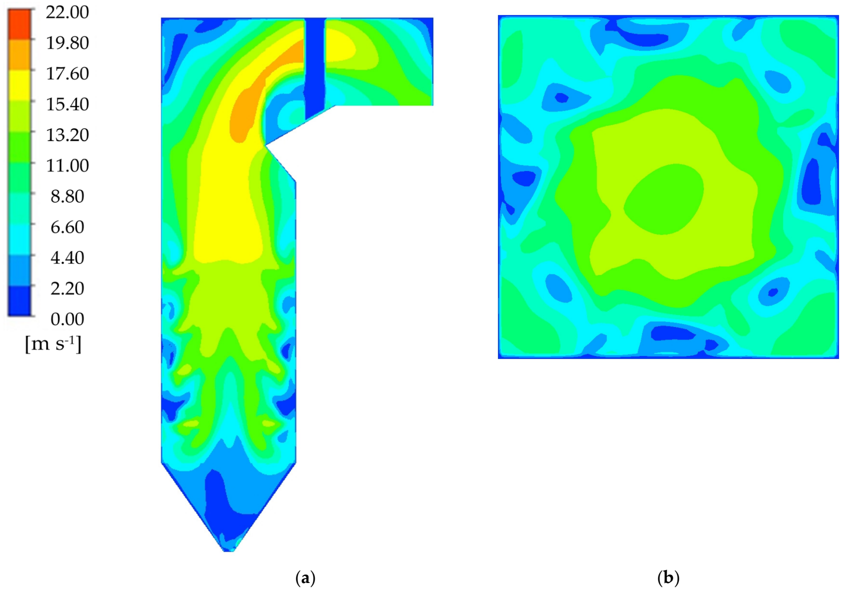

Figure 5. Flow field in the boiler (w = 0). (**a**) Longitudinal section. (**b**) Cross-section.

Figure 6 illustrates the streamlines of the flow emanating from the burner nozzles. The desiccant carrying pulverized coal particles is introduced into the boiler via eight rows of nozzles, resulting in the formation of extensive tangential circles within the central region of the boiler due to the interaction of gas flow. The generation of a tangential circle serves to enhance the residence time of pulverized coal particles, promote the burning of pulverized coal, raise the velocity of flue gas, and strengthen the heat transfer in the boiler [22]. In addition, small vortices appear at the corners between the burners, which is consistent with the phenomenon reported in the literature [36].

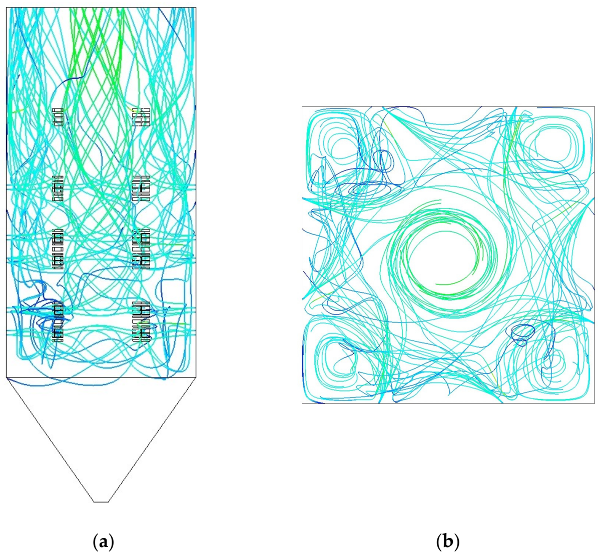

Figure 6. Streamlines in the boiler (w = 0). (**a**) Longitudinal section. (**b**) Cross section.

In the primary combustion zone, the average temperature of the cross-section in the furnace increases with height, as shown in Figure 7. This can be attributed to the fact that the pulverized coal is still in the early stages of combustion, resulting in a lower heat release. Along the height of the furnace, with the continuous addition of pulverized coal and continuous combustion, the rate of heat release increases, causing the temperature within the furnace to rise [37]. The average temperature of the cross-section rises from 1595.5 K at the bottom burners to 1687.8 K at the top burners. In the region between SOFA and the platen bottom, a significant amount of burnout air is introduced, leading to the rapid combustion of any unburned pulverized coal and the release of substantial heat. Therefore, the temperature in this region remains high. At the height of SOFA, the average temperature of the horizontal section is about 1670.8 K, while at the platen bottom, it is 1605.9 K. When the flue gas flows in the horizontal flue, the temperature drops rapidly due to the dense heating surface and the completion of combustion reactions. The flue gas temperature at the boiler outlet is 1144.6 K.

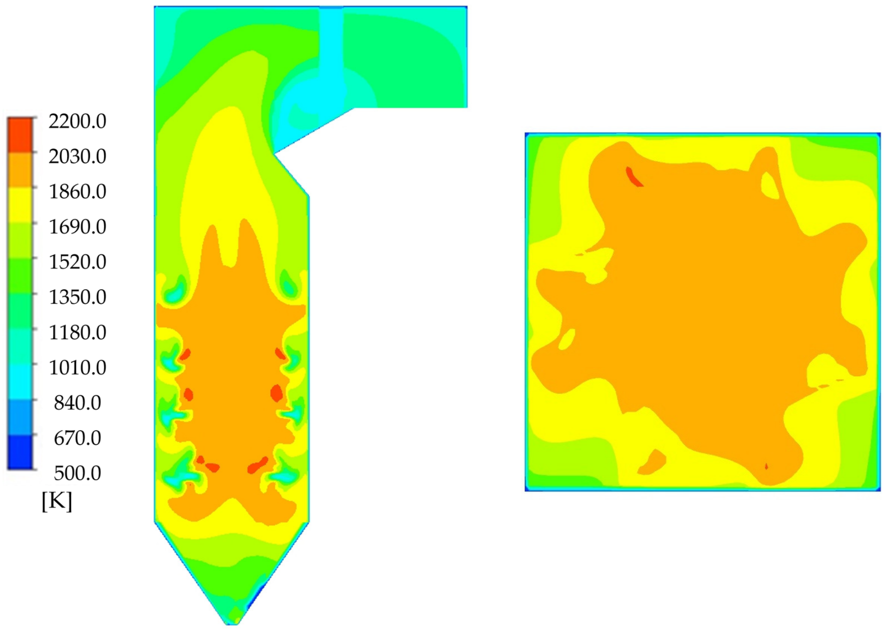

(**a**) (**b**)

Figure 7. Temperature field in the boiler (w = 0). (**a**) Longitudinal section. (**b**) Cross-section.

3.3. Effect of Flue Gas Recirculation Rate

When w increases, the proportion of extracted high-temperature flue gas in the primary combustion zone increases. The hot flue gas is mainly composed of N_2, CO_2, and H_2O, and contains almost no O_2 [38]. Consequently, this leads to a certain degree of reduction in the combustion reaction rate [39]. As shown in Figure 8, when w increases, the mass flow rate of the desiccant through the burner nozzles increases, resulting in an elevated velocity of the flue gas in the primary combustion zone. However, since the quantity of air and coal entering the boiler remains constant, the flue gas velocity at the boiler outlet remains essentially unchanged.

As shown in Figure 9, when w rises from 0 to 30%, the temperature level in the boiler undergoes a continuous decrease. The maximum temperature in the boiler drops from 2162.8 to 2106.5 K, while the average temperature of the central longitudinal section drops from 1589.0 to 1531.9 K. This can be attributed to two factors. Firstly, the introduction of recirculation increases the amount of flue gas present in the primary combustion zone. Secondly, the decrease in the proportion of oxygen in the total air flow entering the furnace, coupled with the increase in the velocity of the airflow within the furnace [39], slows down the rate of combustion reaction [40].

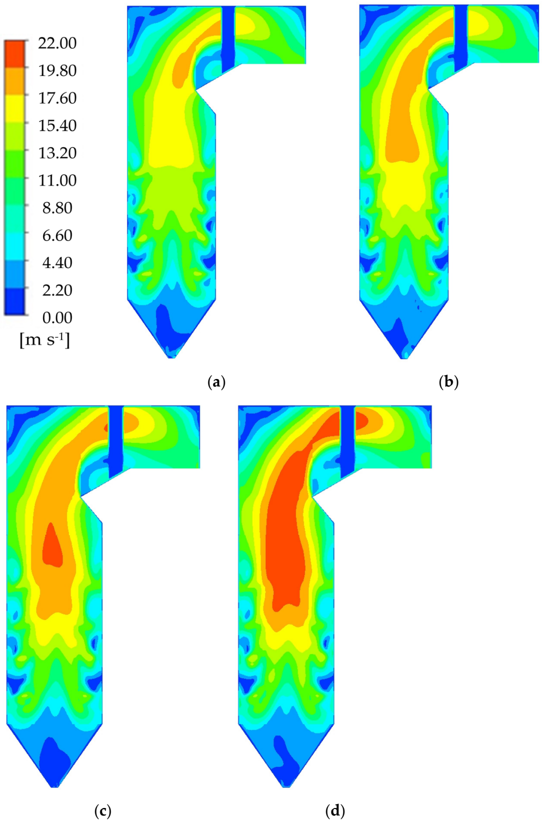

Figure 8. Flow field under different w. (**a**) w = 0. (**b**) w = 10%. (**c**) w = 20%. (**d**) w = 30%.

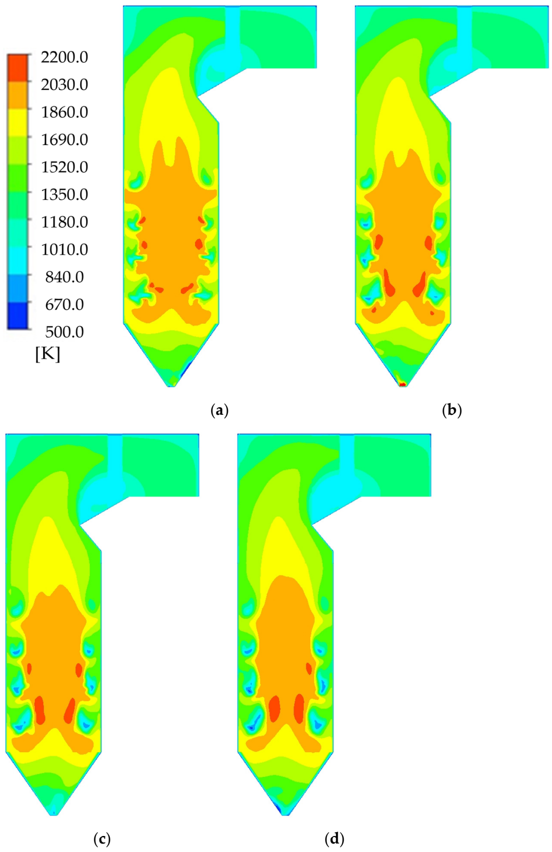

Figure 9. Temperature field under different w. (**a**) w = 0. (**b**) w = 10%. (**c**) w = 20%. (**d**) w = 30%.

With the increase in w, although the flame temperature in the furnace declines, the temperature at the boiler outlet remains relatively stable, as shown in Figure 10. When w increases from 0 to 30%, the flue gas temperature at the boiler outlet only fluctuates between 1144.6 and 1155.5 K, with a maximum deviation of 10.9 K. This means that the overall efficiency of the boiler remains relatively unchanged. However, the flue gas temperature at the platen bottom experiences a noticeable decrease. It decreases from 1605.9 to 1491.9 K. This trend is consistent with findings in the literature [37]. The changing trend of these two quantities indicates that as w increases, the heat absorption of the water-cooled wall decreases, while the heat absorption of the superheater and reheater increases. However, the overall sum of these two heat absorptions remains relatively unchanged.

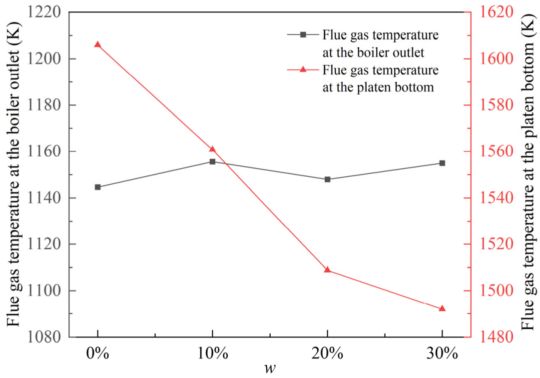

Figure 10. Outlet temperature of the boiler under different w.

Figure 11 can provide a partial explanation for the decrease in temperature level. With the increase in w, two factors contribute to this phenomenon. Firstly, the speed of the pulverized coal flow increases. Secondly, the proportion of oxygen in the primary air decreases. Thus, the combustion reaction is slowed down [39]. This leads to an expansion of the area with a higher mass fraction of O_2. The delayed release of reaction heat due to the slower combustion reaction results in a decrease in the temperature level.

Flue gas recirculation has been proven to be an effective method for reducing NO_x emissions. This is mainly attributed to the addition of recirculated flue gas, which lowers the average temperature in the main combustion zone and reduces oxygen concentration, effectively inhibiting the formation of thermal NO_x. As shown in Figure 12, there is a continuous decrease in the mass fraction of NO_x in the furnace with the increase in w. Specifically, when w increases from 0 to 30%, the mass fraction of NO_x at the furnace outlet decreases from 0.032% to 0.023%. Furthermore, Figure 13 demonstrates that flue gas recirculation also suppresses the generation of CO, which can be explained by Figure 11. Delayed oxygen consumption allows areas with high O_2 content in the furnace to expand. The presence of oxygen enhances the oxidizing atmosphere, resulting in a lower mass fraction of CO. When w increases from 0 to 30%, the average CO mass fraction in the main combustion zone decreases from 0.30% to 0.22%.

3.4. Effect of Biomass Blending Ratio

When w = 20% and r increases, the overall shape of the velocity contours in different working conditions remains similar. However, the velocity level slightly decreases, especially in the region above SOFA. This can be attributed to the fact that the ratio of the theoretical flue gas volume to the lower caloric value of biomass is smaller than that of lignite, with values of 0.30 and 0.43 Nm^3 kJ^{-1}, respectively. This indicates that when blending biomass, the generated flue gas volume is lower than without blending, despite having the same calculated heat input to the boiler. Consequently, with a reduced flue gas volume in the furnace, especially in the upper region, the flow rate of the flue gas in that area also decreases, as shown in Figure 14.

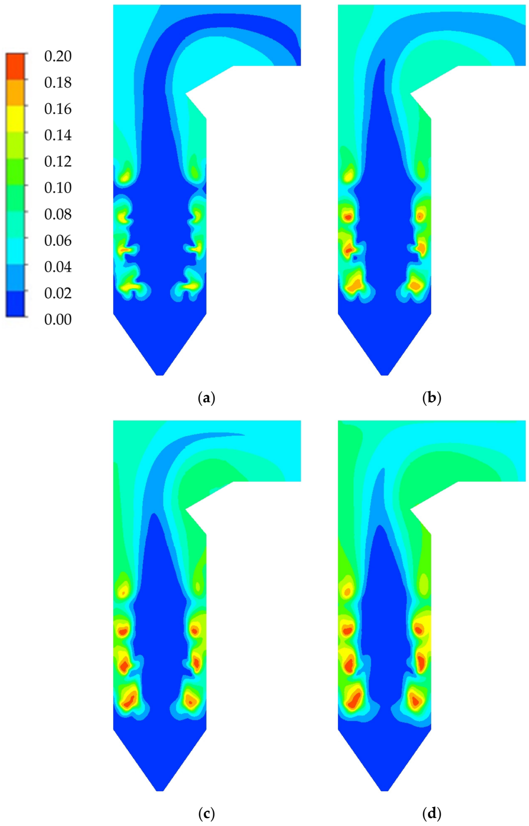

Figure 11. Mass fraction distribution of O_2 under different w. (**a**) w = 0. (**b**) w = 10%. (**c**) w = 20%. (**d**) w = 30%.

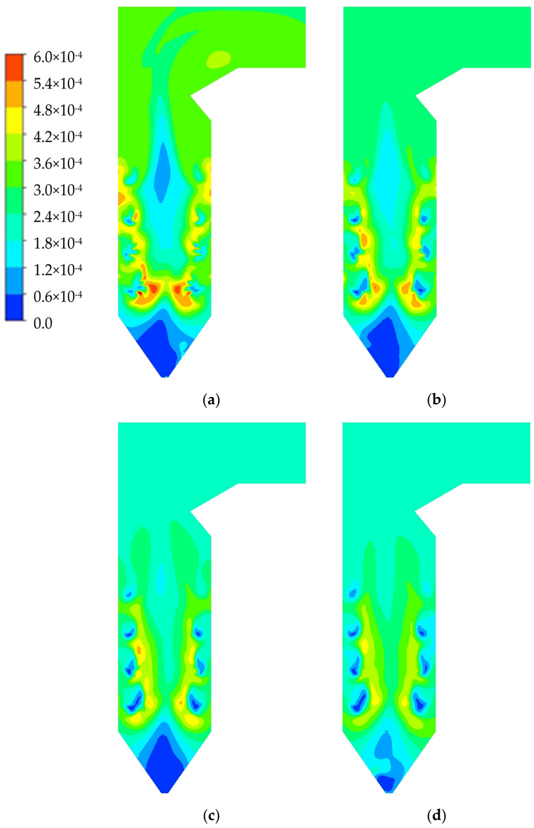

Figure 12. Mass fraction distribution of NO under different w. (**a**) w = 0. (**b**) w = 10%. (**c**) w = 20%. (**d**) w = 30%.

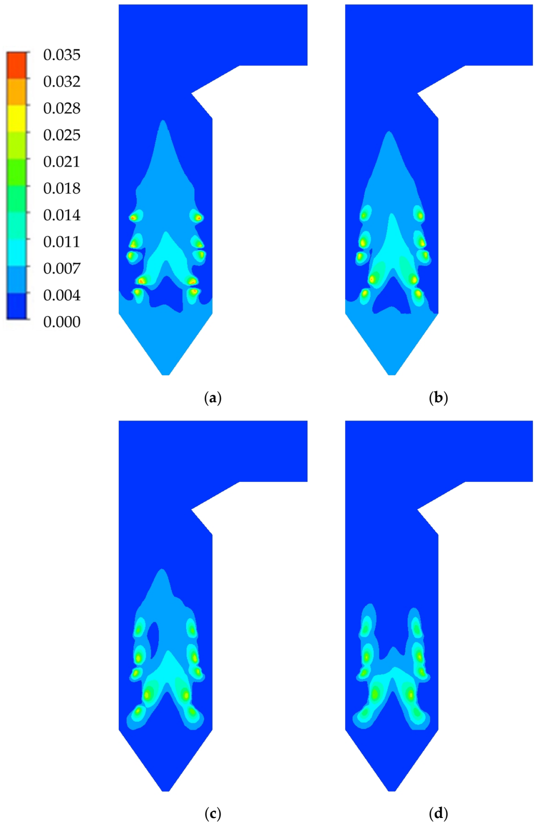

Figure 13. Mass fraction distribution of CO under different w. (**a**) w = 0. (**b**) w = 10%. (**c**) w = 20%. (**d**) w = 30%.

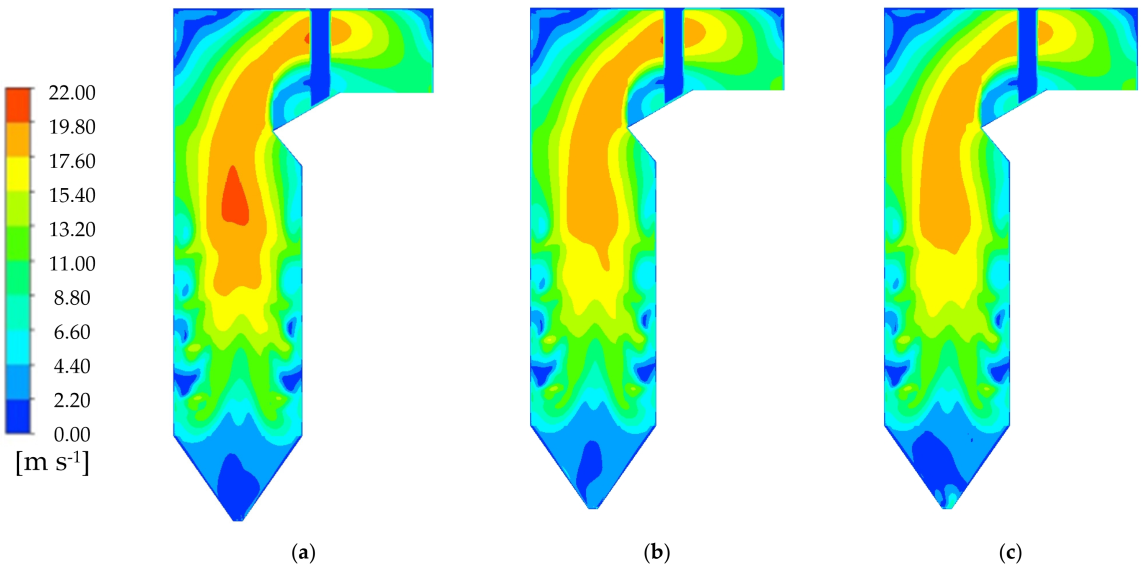

Figure 14. Flow field under different r. (**a**) r = 0. (**b**) r = 10%. (**c**) r = 20%.

When w = 20%, the temperature level of the furnace continuously decreases as r increases, as shown in Figure 15. When r increases from 0 to 20%, the volume mean temperature of the primary combustion zone decreases from 1600.5 to 1571.2 K. This trend is consistent with the literature [14]. The decrease in temperature can be attributed to the drying effect of the recirculated flue gas on lignite. As a result, the energy density of the lignite entering the furnace surpasses that of the industrial analysis. Therefore, the chemical energy carried by corn straw is relatively low. Consequently, the overall temperature within the furnace drops. Additionally, biomass has a tendency to burn more rapidly compared to lignite, resulting in a shorter distance traveled during combustion. As a result, the temperature in the central area of the boiler experiences a decrease.

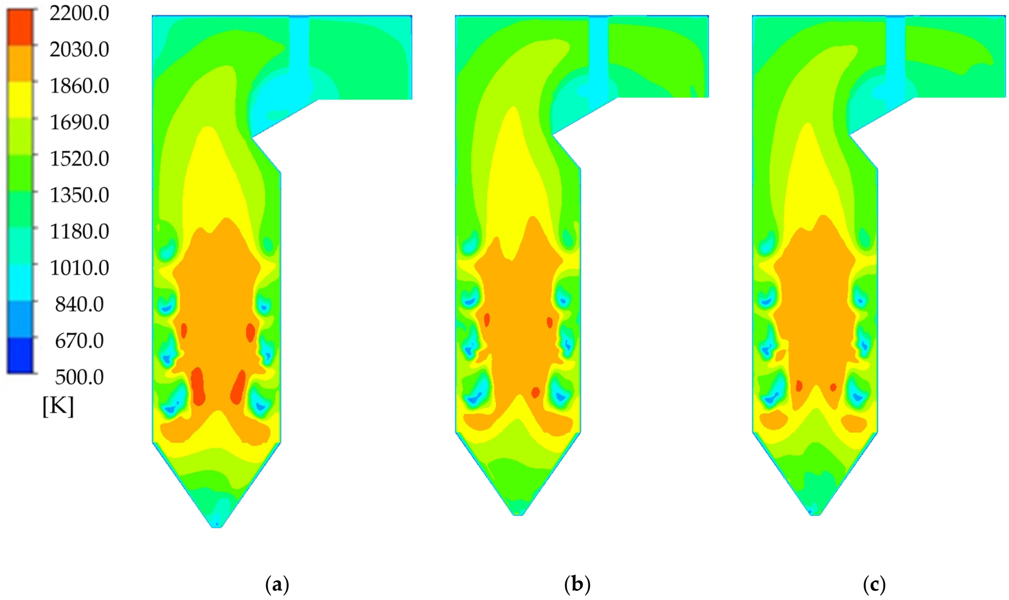

Figure 15. Temperature field under different r. (**a**) r = 0. (**b**) r = 10%. (**c**) r = 20%.

4. Conclusions

A numerical simulation was conducted on an octagonal tangentially fired boiler. The heat and mass transfer in the furnace under the BRL condition was studied in detail. The changes in the combustion characteristic in the furnace were analyzed when the gas recirculation rate and biomass blending ratio changed. The conclusions can be drawn as follows:

1. The air flow from the eight rows of nozzles forms a wide range of tangential circles in the boiler. The flue gas temperature in the primary combustion zone increases with height. From the bottom burners to the top burners, the average temperature of the cross-section rises from 1595.5 to 1687.8 K. At the platen bottom, this temperature is 1605.9 K.
2. Increasing the FGR rate does not significantly alter the flow field in the furnace, but it clearly results in a decrease in the temperature level. When the FGR rate increases from 0 to 30%, the maximum temperature in the furnace decreases by 56.3 K. Meanwhile, the average temperature of the center longitudinal section decreases by 57.1 K.
3. When w increases from 0 to 30%, the maximum deviation of the outlet flue gas temperature in the four calculated working conditions is only 10.9 K. Therefore, the boiler efficiency remains basically unchanged. However, there is a significant decrease in the flue gas temperature at the platen bottom, dropping from 1605.9 to 1491.9 K. It is necessary to consider the heat absorption distribution of each heating surface.
4. The temperature level of the furnace continuously decreases as the biomass blending ratio increases. When the biomass blending ratio increases from 0 to 20%, the average temperature in the main combustion zone decreases from 1600.5 to 1571.2 K. Concurrently, the temperature in the central area of the boiler also decreases.

Author Contributions: Conceptualization, J.D. and J.Y.; methodology, Q.G. and J.D.; validation, J.Y. and Y.Z.; formal analysis, Y.D.; investigation, Y.D. and D.C.; resources, D.C.; data curation, J.Y.; writing—original draft preparation, J.D.; writing—review and editing, J.Y. and Y.Z.; supervision, J.D.; project administration, D.C.; funding acquisition, Q.G., Y.Z. and J.D. All authors have read and agreed to the published version of the manuscript.

Funding: This research was funded by the Shenhua Shendong Power Co., Ltd. 2023 Science and Technology Innovation Project, grant number GSKJ-23-46.

Data Availability Statement: The data presented in this study are available on request from the corresponding author. The data are not publicly available due to privacy.

Conflicts of Interest: The authors declare no conflicts of interest. The funders had no role in the design of the study; in the collection, analyses, or interpretation of data; in the writing of the manuscript; or in the decision to publish the results.

References

1. Hassan, A.; Ilyas, S.Z.; Jalil, A.; Ullah, Z. Monetization of the environmental damage caused by fossil fuels. *Environ. Sci. Pollut. Res.* **2021**, *28*, 21204–21211.
2. Mason, L.R.; Melton, C.C.; Gray, D.; Swallow, A.L. Climate change, social work, and the transition away from fossil fuels: A scoping review. *Sustainability* **2022**, *14*, 7086.
3. Brown, M.; Kearley, V. Role of wood waste as source of biomass fuel in the UK. *Energy Mater.* **2012**, *4*, 162–165.
4. Guan, R.; Yuan, H.; Yuan, S.; Yan, B.; Zuo, X.; Chen, X.; Li, X. Current development and perspectives of anaerobic bioconversion of crop stalks to Biogas: A review. *Bioresour. Technol.* **2021**, *349*, 126615. [CrossRef] [PubMed]
5. Yorifuji, R.; Obara, S.Y. Economic design of artificial light plant factories based on the energy conversion efficiency of biomass. *Appl. Energy* **2022**, *305*, 117850. [CrossRef]
6. Pulles, T.; Gillenwater, M.; Radunsky, K. CO_2 emissions from biomass combustion accounting of CO_2 emissions from biomass under the UNFCCC. *Carbon Manag.* **2022**, *13*, 181–189.
7. Zhang, C.; Nie, J.; Yan, X. Estimation of biomass utilization potential in China and the impact on carbon peaking. *Environ. Sci. Pollut. Res.* **2023**, *30*, 94255–94275. [CrossRef]
8. Dong, K.; Zhang, H.; Tan, H.; Zhang, J.; Hu, Z.; Cheng, Z.; Zhou, Y.; Wang, X. Numerical simulation of biomass high-ratio co-firing in a pre-pyrolysis pulverized coal industrial boiler. *J. China Coal Soc.* **2023**, *48*, 1395–1402.
9. Karampinis, E.; Grammelis, P.; Agraniotis, M.; Violidakis, I.; Kakaras, E. Co-firing of biomass with coal in thermal power plants: Technology schemes, impacts, and future perspectives. *Wiley Interdiscip. Rev. Energy Environ.* **2014**, *3*, 384–399.
10. Król, K.; Nowak-Woźny, D.; Moroń, W. Study of ash sintering temperature and ash deposition behavior during co-firing of polish bituminous coal with barley straw using non-standard tests. *Energies* **2023**, *16*, 4424.
11. Choi, M.; Li, X.; Kim, K.; Sung, Y.; Choi, G. Detailed in-furnace measurements in a pulverized coal-fired furnace with combined woody biomass co-firing and air staging. *J. Mech. Sci. Technol.* **2018**, *32*, 4517–4527. [CrossRef]
12. Taehyun, K.; Won, Y. Influence of biomass co-firing on a domestic pulverized coal power plant in terms of CO_2 abatement and economical feasibility. *J. Korean Soc. Combust.* **2017**, *22*, 14–22.
13. Cutz, L.; Berndes, G.; Johnsson, F. A techno-economic assessment of biomass co-firing in Czech Republic, France, Germany and Poland. *Biofuel. Bioprod. Bior.* **2019**, *13*, 1289–1305.
14. Sun, J.; Zhao, X.; Xue, D. Computational fluid dynamics modeling of biomass co-firing in a 300 MW pulverized coal furnace. *Therm. Sci.* **2022**, *26*, 4179–4191. [CrossRef]
15. Che, D. *Boilers-Theory, Design and Operation*; Xi'an Jiaotong University Press: Xi'an, China, 2008.
16. Kolovos, N.; Sotiropoulos, D.; Georgakopoulos, A. Contribution on lignite recovery from multi-seam deposits. *Energy Sources* **2005**, *27*, 975–986.
17. BP, p.l.c. *BP Statistical Review of World Energy*; BP Press: London, UK, 2022.
18. Hu, L.; Wang, G.; Wang, Q. Efficient drying and oxygen-containing functional groups characteristics of lignite during microwave irradiation process. *Dry. Technol.* **2018**, *36*, 1086–1097.
19. Li, Y.L.; Chen, X.; Zhang, C.Q.; Li, X.F.; Liu, P.; Chen, W.X.; Ren, S.X.; Lei, T.Z. Preparation and structural analysis of humic acid by co-thermal oxidation of wheat straw and Heilongjiang lignite. *J. Fuel Chem. Technol.* **2023**, *51*, 145–154.
20. Zhou, F.; Cheng, J.; Wang, A.; Liu, J.; Zhou, J.; Cen, K. Enhancing slurryabilities of five lignites from Inner Mongolia of China by microwave irradiation. *Dry. Technol.* **2018**, *36*, 100–108.
21. Gurel, B.; Kurtulus, K.; Yurdakul, S.; Dolgun, G.K.; Akman, R.; Onur, M.E.; Varol, M.; Kecebas, A.; Gurbuz, H. Combustion of chicken manure and Turkish lignite mixtures in a circulating fluidized bed. *Renew. Sustain. Energy Rev.* **2024**, *189*, 113960. [CrossRef]
22. Guerel, B.; Kurtulus, K.; Yurdakul, S.; Varol, M.; Kecebas, A.; Gurbuz, H. Numerical and experimental investigation of co-combustion of chicken manure and lignite blends in a CFBB with novel compact combustion chamber. *Energy* **2023**, *285*, 129482.
23. Markovic, J.Z.B.Z.; Marinkovic, A.D.; Savic, J.Z.; Mladenovic, M.R.; Eric, M.D.; Markovic, Z.J.; Ristic, M.D. Risk Evaluation of Pollutants Emission from Coal and Coal Waste Combustion Plants and Environmental Impact of Fly Ash Landfilling. *Toxics* **2023**, *11*, 396. [CrossRef] [PubMed]
24. Chai, W.; Wang, W.; Huang, Y.; Han, G.; Cao, Y.; Liu, J. Further exploring on aqueous chemistry of micron-sized lignite particles in lignite–water slurry: Effects of humics adsorption. *Fuel Process. Technol.* **2018**, *176*, 190–196. [CrossRef]
25. Gu, S.; Xu, Z.; Ren, Y.; Chai, Z.; Zhang, Y. Effect of lignite semi-coke on lignite microwave upgrade and its slurry ability. *Energ. Source Part A* **2023**, *45*, 6442–6455. [CrossRef]

26. Hou, X.; Duan, H.; He, R.; Zhou, H.; Ban, Y.; Li, N.; Zhi, K.; Song, Y.; Liu, Q. Effect of ionic liquids on the microstructure and combustion performance of Shengli lignite. *RSC Adv.* **2023**, *13*, 23669–23681. [CrossRef] [PubMed]
27. Zhang, T.; Lou, C.; Teng, D.; Li, G.; Li, P.; Yun, Q.; Zhou, G. Hot-air drying behavior of lignite and quantitative characterization for its surface damage. *Dry. Technol.* **2023**, *41*, 2171–2188.
28. Nikolopoulos, N.; Agraniotis, M.; Violidakis, I.; Karampinis, E.; Nikolopoulos, A.; Grammelis, P.; Papapavlou, C.; Tzivenis, S.; Kakaras, E. Parametric investigation of a renewable alternative for utilities adopting the co-firing lignite/biomass concept. *Fuel* **2013**, *113*, 873–897.
29. Milicevic, A.; Belosevic, S.; Crnomarkovic, N.; Tomanovic, I.; Stojanovic, A.; Tucakovic, D.; Deng, L.; Che, D. Numerical study of co-firing lignite and agricultural biomass in utility boiler under variable operation conditions. *Int. J. Heat Mass Transf.* **2021**, *181*, 121728. [CrossRef]
30. Adamczyk, W.P. Application of the numerical techniques for modelling fluidization process within industrial scale boilers. *Arch. Comput. Methods Eng.* **2017**, *24*, 669–702.
31. Echi, S.; Bouabidi, A.; Driss, Z.; Abid, M.S. CFD simulation and optimization of industrial boiler. *Energy* **2019**, *169*, 105–114.
32. Zhu, M.; Lu, H.; Zhao, W.; Huang, S.; Chang, X.; Dong, L.; Kong, D.; Jing, X. A numerical study of ash deposition characteristics in a 660mw supercritical tangential boiler. *Adv. Theory Simul.* **2023**, *6*, 2300133.
33. Cheng, S.; Kuang, M.; Liu, S.; Qi, S. Lowering further NOx emissions and improving the hopper's overheating environment in a low-NOx down-fired furnace by a staged arch-firing framework with a primary-burner flue gas recirculation. *Case Stud. Therm. Eng.* **2023**, *51*, 103546.
34. Jiang, Y.; Park, K.-H.; Jeon, C.-H. Feasibility study of co-firing of torrefied empty fruit bunch and coal through boiler simulation. *Energies* **2020**, *13*, 3051.
35. Zhou, Y.; Xu, T.; Hui, S.; Zhang, M. Experimental and numerical study on the flow fields in upper furnace for large scale tangentially fired boilers. *Appl. Therm. Eng.* **2009**, *29*, 732–739.
36. Drosatos, P.; Nikolopoulos, N.; Agraniotis, M.; Kakaras, E. Numerical investigation of firing concepts for a flexible Greek lignite-fired power plant. *Fuel Process. Technol.* **2016**, *142*, 370–395. [CrossRef]
37. Deng, L.; Dong, L.; Bai, Y.; Wu, Y.; Liu, H.; Belošević, S.; Tomanović, I.; Che, D. Effects of flue gas recirculation on combustion and heat flux distribution in 660 MW double-reheat tower-type boiler. *Fuel* **2022**, *321*, 123988.
38. Ishihara, S.; Zhang, J.; Ito, T. Numerical calculation with detailed chemistry of effect of ammonia co-firing on NO emissions in a coal-fired boiler. *Fuel* **2020**, *266*, 116924.
39. Gu, M.; Yuan, J.; Wang, M.; Wang, J.; Huang, X.; Chu, H. Effects of flue gas recirculation on nitrogen oxide formation in 1000 MW S-CO_2 coal-fired boiler with partial expansion furnace. *Int. J. Chem. React. Eng.* **2022**, *20*, 929–945. [CrossRef]
40. Zhu, Y.; Wang, C.; Chen, X. Combustion characteristic study with a flue gas internal and external double recirculation burner. *Chem. Eng. Process.* **2021**, *162*, 108345.